*Cerebral Cortex*, February 2019;29: 765–776

**doi: 10.1093/cercor/bhx358**
Advance Access Publication Date: 20 January 2018
Original Article

ORIGINAL ARTICLE

# Neonatal Hypoxia–Ischemia Causes Functional Circuit Changes in Subplate Neurons

Aminah Sheikh[1,2,†], Xiangying Meng[1,†], Ji Liu[1], Alexandra Mikhailova[4], Joseph P. Y. Kao[3], Patrick S. McQuillen[4] and Patrick O. Kanold[1,2]

[1]Department of Biology, University of Maryland, College Park, MD 20742, USA, [2]Neuroscience and Cognitive Science Program, University of Maryland, College Park, MD 20742, USA, [3]Center for Biomedical Engineering and Technology, and Department of Physiology, University of Maryland School of Medicine, Baltimore, MD 21201, USA and [4]Departments of Pediatrics and Neurology, University of California, San Francisco, CA 94143, USA

Address correspondence to Patrick O. Kanold, Department of Biology, University of Maryland, 1116 Biosciences Res. Bldg, College Park, MD 20742, USA. Email: pkanold@umd.edu

[†]These authors contributed equally.

## Abstract

Neonatal hypoxia–ischemia (HI) in the preterm human results in damage to subcortical developing white matter and cognitive impairments. Subplate neurons (SPNs) are among the first-born cortical neurons and are necessary for normal cerebral development. While moderate or severe HI at P1 in rats leads to SPN loss, it is unclear if HI, esp. forms not associated with overt cell loss lead to altered SPN circuits. Thus, we used two HI models with different severities in P1 rats. Cauterization of the common carotid artery (CCA) causes a largely transient and thus milder ischemia (HI-Caut) while CCA ligation causes more severe ischemia (HI-Lig). While HI-Lig caused subplate damage, HI-Caut did not cause overt histological damage on the light microscopic level. We used laser-scanning photostimulation (LSPS) in acute thalamocortical slices of auditory cortex during P5–10 to study the functional connectivity of SPNs. Both HI categories resulted in hyperconnectivity of excitatory and inhibitory circuits to SPNs. Thus, alterations on the circuit level are present in the absence of cell loss. Our results show that SPN circuits are uniquely susceptible to HI. Given the key developmental role of SPNs, our results suggest that altered SPN circuits might underlie the abnormal development of cortical function after HI.

**Key words:** auditory cortex, complexin-3, cortical, hypoxia–ischemia, neonatal, subplate

## Introduction

Early birth or disruptions of prenatal brain development result in increased risk of cognitive impairments. For example, hypoxic–ischemic (HI) brain injuries disrupt normal maturation and consequently increases the risk of developing cerebral palsy and epilepsy in infants (du Plessis and Volpe 2002; Ferriero 2004; Volpe 2012). Rodent models of HI show that sensory evoked activity and plasticity in sensory cortices are impaired consequent to HI (Failor et al. 2010; Ranasinghe et al. 2015), suggesting that underlying cortical circuits might have changed. However, it is unclear which specific circuits are affected by HI, and how this change translates to reduced overall network activity.

One important neuronal circuit present in early cortical development is formed by subplate neurons (SPNs). SPNs are a largely transient neuronal population that is highly overrepresented in humans (Kostovic and Rakic 1990; Kanold and Luhmann 2010; Judas et al. 2013). SPNs receive thalamic inputs (Friauf et al. 1990; Higashi et al. 2005; Zhao et al. 2009), respond

to early sensory stimuli (Wess et al. 2017), and excite developing layer 4 neurons (Zhao et al. 2009; Deng et al. 2017). Thus, at early ages SPNs provide a relay of thalamic information to the developing cortical plate. Since SPNs also receive functional inputs from the developing cortical plate (Viswanathan et al. 2012; Meng et al. 2014), SPNs integrate early ascending information from the thalamus with ongoing activity in the cortical plate.

SPN ablations in early development have been shown to result in a variety of deficits on both anatomical and functional levels. SPN ablations prevented the functional and anatomical maturation of thalamocortical circuits, the development of sensory responses, and altered plasticity during the critical period (Kanold et al. 2003; Kanold and Shatz 2006; Tolner et al. 2012).

HI injuries, in particular those of higher severity, cause a loss of a fraction of SPNs labeled with bromodeoxyuridine (BrdU) at their birth (McQuillen et al. 2003; Failor et al. 2010) suggesting that SPNs are vulnerable to HI performed at ~P1 (McQuillen et al. 2003; McQuillen and Ferriero 2005; Millar et al. 2017). Such early HI injury also leads to abnormal functional cortical responses at later ages (Failor et al. 2010; Ranasinghe et al. 2015), which were reminiscent of the consequences of SPN ablations including altered sensory responses and cortical oscillatory patterns (Kanold et al. 2003; Kanold and Shatz 2006; Tolner et al. 2012). Together these HI studies in rodent suggested that HI led to SPN abnormalities which in turn prevented normal development of functional responses.

Normal functional responses in sensory cortices depend on mature thalamocortical and intracortical circuits. While the effects of moderate to severe HI on the numbers of SPNs neurons have been established, how milder injuries lead to functional changes at later ages has not been established. In particular, besides SPN loss observed in moderate to severe cases of HI, milder forms of HI could cause functional changes in SPN circuits. To identify such functional changes, we investigated the effects of HI on intracortical circuits to SPNs.

To delineate functional changes from cell loss, we used 2 rat HI models with different severities. Cauterization of the common carotid artery (CCA) caused a largely transient (Segovia et al. 2008) and thus milder form of ischemia (HI-Caut) while ligating the CCA caused a permanent, and thus more severe form of ischemia (HI-Lig). We performed HI at P1 and found that neither HI-Lig nor HI-Caut resulted in gross loss of SPNs.

In humans, HI can cause a disruption of fine and gross motor function, speech, and language development, cerebral palsy and abnormalities in cognitive function (Robertson and Perlman 2006; Lai and Yang 2011; Martinez et al. 2014). We thus here focused on the auditory cortex (ACX). To determine if either form of HI has effects beyond SP lesions, we used laser-scanning photostimulation (LSPS) to analyze the functional spatial connection patterns of SPNs during postnatal day (P) 5–10 in a thalamocortical slice preparation of ACX. Both HI-Caut and HI-Lig caused hyperconnectivity of excitatory and inhibitory connections to SPNs. These results show that functional changes were present in the absence of histological SPN loss. Together these results suggest that SPNs are injured by HI, and that disruptions of SPN circuits may lead to the abnormal cortical function observed after HI.

Preliminary results were presented in abstract form (Sheikh et al. 2017).

## Methods

All procedures were approved by the University of Maryland Institutional Animal Care and Use Committee.

### Animals

Timed-pregnant Sprague–Dawley rats were obtained from Charles River. Time of birth was marked P0 (±0.5 day).

### Hypoxia–Ischemia

Sprague–Dawley pups at postnatal day (P) 1–2 were anesthetized with 2–4% isoflurane for the Rice-Vannucci procedure (McQuillen et al. 2003; Failor et al. 2010; Ranasinghe et al. 2015). A small incision was made in the midline of the neck just above the sternal notch. The common carotid artery (CCA) was exposed and coagulated. Care was taken not to damage the sympathetic ganglion chain in order to avoid Horner's Syndrome, which results in ptosis. Different surgical techniques were used to cause ischemia of different severities. Cauterization of the CCA caused a largely transient and thus milder form of ischemia (HI-Caut). Alternatively, ligating the CCA with a single suture caused a permanent, and more severe form of ischemia (HI-Lig). Sham surgeries exposing the CCA were performed as a control. Because the common carotid artery is proximal to the circle of Willis, both techniques only cause partial ischemia.

After recovery, the pups were returned to the dam in normal room air for 2 h. Following recovery, the pups were placed in humidified chambers (Lexan, UMD Physics shop) and exposed to 5% oxygen (concentration monitored in chamber by UV Flux 25% Oxygen Sensor Module CM-0201, co2meter.com; GasLab® software), balanced nitrogen for 2–3 h and then returned to the dam. Chamber temperature was held constant by a water bath. During hypoxia, one pup from each litter was monitored for skin temperature. Skin temperature was kept constant at 35 °C. Surviving pups were removed if the total mortality rate for the entire litter reached 30–50% on average. Chambers remained closed until the end of the hypoxia procedure.

### Cortical Thickness Analysis

Animals were deeply anesthetized with isoflurane and were perfused transcardially with 4% paraformaldehyde (PFA). When brains were removed, the right hemisphere of the brain was cut below the rhinal fissure to retain the identity of the ischemic hemisphere throughout histology experiments. Brains were postfixed overnight in 4% PFA at 4 °C, transferred to 30% sucrose in PBS, and coronal sections (50 μm) were cut on a freezing sliding microtome. Nissl staining allowed for identification of cortical layers including the subplate and the ventricular boundaries. Free-floating 50 μm coronal sections were rinsed in PBS, mounted and stained with cresyl violet. Slides were scanned at 1× (Nikon Super Coolscan 9000ED) and cortical thickness was measured in MATLAB. Measurements were taken from pia to ventricle. We calculated the ratio of the extent of auditory cortex (ACX) in both hemispheres. The location of the measured area of ACX was identified by the position relative to the hippocampus. We then averaged the ratios from all slices from each brain. Brains from each condition (Control, HI-Caut, and HI-Lig) were measured for cortical shrinkage. (Control, $N = 5$ brains, 24 slices total; HI-Caut, $N = 14$ brains, 36 slices total; HI-Lig, $N = 5$ brains, 19 slices total)

### Quantification of Infarct Volume

Quantification of infarct volume was performed as described previously (Ranasinghe et al. 2015; Mikhailova et al. 2017). Paraformaldehyde perfusion fixed brains were cryoprotected and sectioned on a freezing sliding microtome at 80 μm. For

Nissl staining, every 12th section was collected and mounted on a slide, and then stained with cresyl violet. We used the Cavalieri method (StereoInvestigator) on Nissl stained sections to evaluate hemispheric volumes of 3 groups of animals: Control, HI-ligated, HI-cauterized. Infarct volume ratios are defined as (hypoxia hemisphere − HI hemisphere)/hypoxia hemisphere × 100. Ventricles were excluded from the tracing area.

### Immunofluorescence

For complexin-3 immunostaining, sections were blocked (5% donkey serum, 10% BSA, 5% fish skin gelatin, and 0.1% Triton X-100 in 0.1 M phosphate-buffered saline) and then incubated overnight with anti-Complexin-3 antibody (1:1000; rabbit polyclonal, 122 302, Synaptic Systems). Following primary incubation and washing, sections were incubated with secondary antibody (1:500; donkey antirabbit labeled with AlexaFluor488; Jackson) and counterstained with DAPI (PureBlu™; BioRad). Sections were imaged using Zeiss Axioscope II Epifluorescence microscope at ×10.

### Brain Slice Preparation and Solutions

Thalamocortical brain slices were prepared as previously described for mice (Zhao et al. 2009; Viswanathan et al. 2012; Meng et al. 2014). Rats of either sex were used. Rats were deeply anesthetized with isoflurane prior to decapitation and removal of the brain. Acute thalamocortical slices (500 μm) were prepared using a vibrating microtome (Leica) in ice-cold artificial cerebral spinal fluid (ACSF) consisting of (in mM): 130 NaCl, 3 KCl, 1.25 $NaH_2PO_4$, 20 $NaHCO_3$, 10 glucose, 1.3 $MgSO_4$, 2.5 CaCl, pH 7.35–7.4, equilibrated with 95% $O_2$–5% $CO_2$. The slices were incubated in ACSF for 1 h at 30 °C and then kept at room temperature.

### Electrophysiology

Whole-cell recordings were performed on P5–10 subplate neurons with a patch-clamp amplifier (Multiclamp 700B; Molecular Devices). Electrodes were filled with (in mM): 115 cesium methanesulfonate ($CsCH_3SO_3$), 5 NaF, 10 EGTA, 15 CsCl, 3.5 MgATP, 3 QX-314, pH 7.25, 300 mOsm. Biocytin or Neurobiotin (0.5%) was added to the electrode solution as needed. To reduce the probability of multi-synaptic events, all slices are perfused during recording with a high-$Mg^{2+}$ ACSF solution: 124 NaCl, 5 KCl, 1.23 $NaH_2PO_4$, 26 $NaHCO_3$, 10 glucose, 4 $MgCl_2$, 4 $CaCl_2$. The electrode resistance in the bath was 4–10 MΩ. Data were acquired with a National Instruments AD board and software EPHUS (Suter et al. 2010). Membrane voltages were corrected for an estimated liquid junction potential of 10 mV. Soma activation profiles of neurons were created by recording in loose-patch mode while mapping the same area and recording action potentials.

### Dendritic Morphological Analysis

Recorded cells filled with Biocytin were stained and reconstructed in Neurolucida (MBF Bioscience). Sholl analysis was performed in Neurolucida.

### Laser-scanning Photostimulation (LSPS)

LSPS was performed as previously described (Viswanathan et al. 2012; Meng et al. 2014). 0.5–1 mM caged glutamate (Ncm-Glu [*N*-(6-nitro-7-coumarylmethyl-L-glutamate)]) (Kao 2006; Muralidharan et al. 2016) was added to the ACSF. We typically stimulated an array of up to 30 × 30 sites with 40 μm spacing to enable us to probe areas of ~1 mm × 1 mm. Stimuli were applied at 1 Hz. Laser power (<25 mW) was adjusted to achieve reliable neuron activation and reproducible maps. The same settings were used through all experiments. To detect monosynaptically evoked EPSCs, we measured peak EPSC amplitudes in a 50 ms time window after the stimulation. AMPAR-mediated responses were recorded by holding cells at −70 mV, while GABA-mediated responses were recorded at a 0 mV holding potential. Traces containing a short-latency (~8 ms) response were considered to result from direct activation of receptors on the patched cell and were excluded from analysis. Traces with latencies longer than 50 ms were discarded due to potential involvement of polysynaptic components. Analysis was performed essentially as previously described with custom software written in MATLAB (Meng et al. 2014). Layer boundaries were determined from infrared images as previously described (Meng et al. 2014).

### Statistics

Results are analyzed by using the Multiple Comparison test. To perform multiple comparison of group means, we used one-way ANOVA or Kruskal–Wallis test based upon normality of the data. Histology analysis results are plotted as boxplots using two-sided Student's *t*-test or one-way ANOVA (normally distributed).

## Results

### Mild Neonatal HI Does Not Cause SPN Loss

We sought to investigate the influence of HI on SPN circuits. Since the effects on SPNs and other neurons might depend on the amount of injury, we investigated the effect of different amounts of injury by utilizing two different surgical techniques to induce the ischemia: cauterization or ligation of the CCA. Cauterization causes a reversible ischemia (HI-Caut), while ligation causes permanent ischemia (HI-Lig). Thus, the latter procedure is likely to induce a more severe damage than the former. We performed HI at P1-2 because SPNs have been shown to be vulnerable to injury at these ages (McQuillen et al. 2003; Failor et al. 2010; Ranasinghe et al. 2015; Mikhailova et al. 2017). We first assessed the severity of injury to auditory cortex and selective vulnerability of SPNs resulting from our two different HI procedures on the histological level. Prior studies distinguished 3 categories of brain injury: "mild", "moderate", and "severe" based on cortical shrinkage and loss of SPNs identified by BrdU birthdating (McQuillen et al. 2003; Failor et al. 2010). To evaluate the amount of shrinkage of auditory cortex, we harvested brains at P5–P10 from HI or control animals and used Nissl staining to reveal the extent of the cortical layers in the manipulated and unmanipulated hemispheres (Fig. 1*A*). We found that compared with Control, HI-Caut did not result in significant cortical shrinkage while HI-Lig resulted in cortical shrinkage of similar in degree to the "mild" category (McQuillen et al. 2003; Failor et al. 2010) (Fig. 1*B*). Since cortical shrinkage can result from a variety of causes, we next analyzed injury severity in the two methods in more detail using stereological measurements (Mikhailova et al. 2017). We used a separate cohort of animals ($N = 22$) and compared animals receiving HI or control littermates by an independent group blinded to condition. Injury severity was measured using categorical injury scoring,

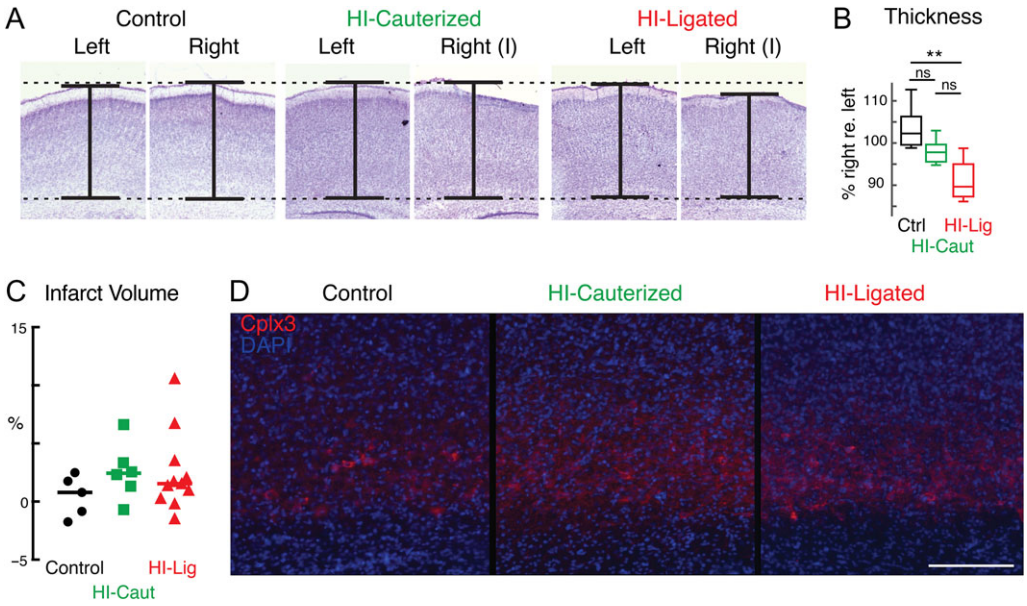


**Figure 1.** Different severities of HI injury. (*A*) Examples of 50 μm coronal Nissl stained slices containing auditory cortex at different severities of hypoxia–ischemia. Slices were measured to obtain thicknesses of cortex. One example of each condition is presented. (*B*) Percentage of cortical thickness in manipulated (right) relative to unmanipulated (left) hemisphere. HI-Caut did not result in statistically significant shrinkage while HI-Lig resulted in significant cortical shrinkage compared with Control ($P = 0.18$ and $P = 0.003$ respectively, ANOVA). (*C*) Stereologic measurement of infarct volume identified by Complexin 3 expression (see Table 1). Hi-Lig produced the largest range of infarct volumes. (*D*) Representative examples of Complexin-3 immunofluorescence (red) staining in presumptive auditory cortex in each condition (Control, HI-Lig, HI-Caut). DAPI nuclear counterstain shown in blue. Scale bar = 200 μm.

**Table 1** Injury severity

| Condition | Injury category % (*N*) | | | Infarct volume (%) median (range) |
|---|---|---|---|---|
| | Mild | Moderate | Severe | |
| Control-Sham | 100% (5) | | | 0.79 (−1.75, 2.49) |
| HI-Cauterized | 100% (6) | | | 2.44 (−0.69, 6.63) |
| HI-Ligated | 82% (9) | 18% (2) | | 1.54 (−1.47, 10.57) |

**Table 2** Values for Figure 2

| % Locations | Control Mean ± SEM (μm) | HI-Lig Mean ± SEM (μm) | P-value |
|---|---|---|---|
| L4 | 214.89 ± 26.08 | 270.12 ± 27.93 | $P = 0.20$ |
| L5/6 | 228.82 ± 16.66 | 297.16 ± 20.68 | $P = 0.43$ |
| SP | 224.73 ± 23.91 | 284.84 ± 22.94 | $P = 0.34$ |
| **Spike count** | **Control** | **HI-Lig** | **P-value** |
| Total cells | 49 | 48 | |
| L4 | 18 | 17 | $P = 0.73$ |
| L5/6 | 15 | 15 | $P = 0.75$ |
| SP | 16 | 16 | $P = 0.07$ |

stereologic measurement of infarct volume, and qualitative assessment of subplate neurons identified by Complexin-3 expression (Hoerder-Suabedissen et al. 2009; Viswanathan et al. 2012, 2016; Mikhailova et al. 2017). Most animals in the HI groups ($N = 15/17$, Table 1) had mild injuries, with no detectable differences in subplate density by Complexin-3 expression (Fig. 1*C*, *D*, Table 1). None of the animals examined had severe injury. While infarct volumes were not significantly different across the groups ($P = 0.6$, Wilcoxon Rank Sum), the ligation method for permanent ischemia produced the largest range of infarct volumes and only two cases with moderate injury severity. In these two cases, HI-Lig appeared to cause greater injury to lower cortical layers (V–VI) than is typically observed with the HI cauterization method, and out of proportion to subplate layer injury. Together these results show that our manipulations did not grossly reduce the numbers of SPNs (Tables 1).

## Both Severities of Neonatal HI Cause Functional Hyperconnectivity in Excitatory Subplate Circuits

So far we have shown that both of our HI methods caused mild injuries with no apparent SPN loss. We next investigated the effects of HI on functional microcircuits impinging on SPNs. We used laser-scanning photostimulation (LSPS) with caged glutamate combined with whole-cell patch-clamp recordings in thalamocortical slices of A1 (Fig. 2*A*) (Shepherd et al. 2003; Meng et al. 2014) to spatially map the connectivity of excitatory (AMPA) and inhibitory (GABA) inputs to primary ACX (A1) SPNs at P5–P10. This age is before the opening of the ear canals and mature thalamocortical transmission to L4 (~P11-12 in the rat) (Zhang et al. 2001; Barkat et al. 2011) and during this timeframe there is a high density of SPNs present (Kanold and Luhmann 2010; Hoerder-Suabedissen and Molnar 2015).

We first assessed if HI altered the sensitivity of neurons across the cortical column to exogenously applied glutamate. Loose-patch or cell-attached recordings ($N = 97$ cells; 49 cells in 9 Control animals; 48 cells in 9 HI-Lig animals) show that the injury did not change the distance from the soma from which action potentials could be elicited (Fig. 2*B*) nor the numbers of action potentials evoked (Fig. 2*C*, Table 2). Our stimulation evoked on average, 1 action potential in targeted cells. Thus, HI did not lead to gross changes in cellular excitability by exogenously applied glutamate, and thus the spatial resolution of the LSPS technique is not altered after HI.

**Table 3** Values for Figure 3

| Total area (E) | Control (S)<br>Mean ± SEM ($\mu m^2$) | HI-Caut (C)<br>Mean ± SEM ($\mu m^2$) | HI-Lig (L)<br>Mean ± SEM ($\mu m^2$) |
|---|---|---|---|
| L4 | $3.00 \times 10^4 \pm 4.52 \times 10^3$ | $2.18 \times 10^4 \pm 4.45 \times 10^3$ | $3.07 \times 10^4 \pm 3.96 \times 10^3$ |
| L5/6 | $8.60 \times 10^4 \pm 7.95 \times 10^3$ | $9.04 \times 10^4 \pm 5.38 \times 10^3$ | $1.18 \times 10^5 \pm 7.21 \times 10^3$ |
| SP | $2.52 \times 10^4 \pm 2.70 \times 10^3$ | $4.17 \times 10^4 \pm 2.96 \times 10^3$ | $4.17 \times 10^4 \pm 2.79 \times 10^3$ |
| Mean charge (F) | Mean ± SEM (pC) | Mean ± SEM (pC) | Mean ± SEM (pC) |
| L4 | 1.91 ± 0.26 | 1.22 ± 0.29 | 1.58 ± 0.24 |
| L5/6 | 4.61 ± 0.44 | 4.61 ± 0.37 | 4.94 ± 0.35 |
| SP | 4.82 ± 0.53 | 4.94 ± 0.45 | 5.63 ± 0.57 |
| Width (G) | Mean ± SEM (μm) | Mean ± SEM (μm) | Mean ± SEM (μm) |
| L4 | 283.47 ± 34.80 | 213.68 ± 35.93 | 316.75 ± 37.91 |
| L5/6 | 415.65 ± 26.91 | 449.47 ± 19.57 | 513.51 ± 22.05 |
| SP | 347.82 ± 29.65 | 421.05 ± 30.46 | 431.35 ± 29.49 |
| Area | Comparison<br>(S–C) | Comparison<br>(S–L) | Comparison<br>(C–L) |
| L4 | $P = 0.53$ | $P = 0.90$ | $P = 0.21$ |
| L5/6 | $P = 0.97$ | $P = 0.02$ | $P = 0.08$ |
| SP | $P = 4.93 \times 10^{-4}$ | $P = 0.06$ | $P = 0.50$ |
| Charge | | | |
| L4 | $P = 0.15$ | $P = 0.75$ | $P = 0.68$ |
| L5/6 | $P = 1.00$ | $P = 0.98$ | $P = 0.98$ |
| SP | $P = 0.98$ | $P = 0.91$ | $P = 0.74$ |
| Width | | | |
| L4 | $P = 0.37$ | $P = 0.87$ | $P = 0.10$ |
| L5/6 | $P = 0.73$ | $P = 0.01$ | $P = 0.23$ |
| SP | $P = 0.29$ | $P = 0.27$ | $P = 0.99$ |

**Table 4** Values for Figure 4

| Total area (E) | Control (S)<br>Mean ± SEM ($\mu m^2$) | HI-Caut (C)<br>Mean ± SEM ($\mu m^2$) | HI-Lig (L)<br>Mean ± SEM ($\mu m^2$) |
|---|---|---|---|
| L4 | $3.00 \times 10^4 \pm 4.52 \times 10^3$ | $2.18 \times 10^4 \pm 4.45 \times 10^3$ | $3.07 \times 10^4 \pm 3.96 \times 10^3$ |
| L5/6 | $8.60 \times 10^4 \pm 7.95 \times 10^3$ | $9.04 \times 10^4 \pm 5.38 \times 10^3$ | $1.18 \times 10^5 \pm 7.21 \times 10^3$ |
| SP | $2.52 \times 10^4 \pm 2.70 \times 10^3$ | $4.17 \times 10^4 \pm 2.96 \times 10^3$ | $4.17 \times 10^4 \pm 2.79 \times 10^3$ |
| Mean charge (F) | Mean ± SEM (pC) | Mean ± SEM (pC) | Mean ± SEM (pC) |
| L4 | 1.91 ± 0.26 | 1.22 ± 0.29 | 1.58 ± 0.24 |
| L5/6 | 4.61 ± 0.44 | 4.61 ± 0.37 | 4.94 ± 0.35 |
| SP | 4.82 ± 0.53 | 4.94 ± 0.45 | 5.63 ± 0.57 |
| Width (G) | Mean ± SEM (μm) | Mean ± SEM (μm) | Mean ± SEM (μm) |
| L4 | 213.91 ± 33.22 | 310.52 ± 49.97 | 287.56 ± 40.35 |
| L5/6 | 339.13 ± 33.99 | 445.26 ± 27.32 | 411.89 ± 35.54 |
| SP | 269.56 ± 31.51 | 426.31 ± 36.37 | 323.24 ± 40.39 |
| Area | Comparison<br>(S–C) | Comparison<br>(S–L) | Comparison<br>(C–L) |
| L4 | $P = 0.38$ | $P = 0.96$ | $P = 0.70$ |
| L5/6 | $P = 0.06$ | $P = 0.32$ | $P = 0.89$ |
| SP | $P = 0.01$ | $P = 0.98$ | $P = 0.06$ |
| Charge | | | |
| L4 | $P = 0.96$ | $P = 0.48$ | $P = 0.25$ |
| L5/6 | $P = 0.07$ | $P = 0.99$ | $P = 0.05$ |
| SP | $P = 0.36$ | $P = 0.94$ | $P = 0.14$ |
| Width | | | |
| L4 | $P = 0.45$ | $P = 0.48$ | $P = 0.99$ |
| L5/6 | $P = 0.10$ | $P = 0.40$ | $P = 0.90$ |
| SP | $P = 8.00 \times 10^{-3}$ | $P = 0.70$ | $P = 0.19$ |

To spatially map the functional synaptic input onto SPNs, we recorded ACX SPNs in thalamocortical slices ($N = 121$ cells; 46 cells in 8 Control animals, 38 cells in 8 HI-Caut animals, and 37 cells in 5 HI-Lig animals). We first held cells at a holding potential of −70 mV to isolate excitatory synaptic inputs. We sequentially targeted 900 (30 × 30) stimulation sites (40 μm spatial resolution) in a pseudorandom pattern (Viswanathan et al. 2012). Our stimulation sites covered the entire radial extent of the cortical column from ventricle to pia (Fig. 2D). If a connection was present between a stimulated neuron and the recorded neuron, a long-latency postsynaptic current (PSC) was revealed (Fig. 2E) (Meng et al. 2014).

We first analyzed the excitatory circuits associated with SPNs by holding cells at −70 mV (Fig. 3A). For stimulation sites that evoked excitatory postsynaptic currents (EPSCs), we measured the size of the EPSC to construct a 2-dimensional map of excitatory connectivity for each cell (Fig. 2F). This map indicates the strengths of the connections from the location of presynaptic cells to the recorded SPN. We then aligned the maps of all recorded SPNs to the soma position and calculated for every spatial location the probability of being connected to a given SPN, resulting in a spatial connection probability map (Fig. 3B) (Meng et al. 2014). Compared with the control, qualitative inspection showed that excitatory input to the recorded SPNs seemed to originate from more distant locations and having higher connection probabilities in HI conditions, possibly indicating hyperconnectivity. While the total cortical area that gave rise to inputs did not show a significant difference after HI (Fig. 3C), laminar analysis showed that both HI conditions caused an increase in the number of excitatory inputs to SPNs (Fig. 3E, Table 3). HI-Caut resulted in an increase in excitatory input from within the subplate, while HI-Lig resulted in a larger total area of excitatory input from Layer 5/6 (L5/6) to SPNs (Fig. 3E). In contrast, the mean EPSC charge of the laminar inputs did not vary (Fig. 3D, F; Table 3).

Our results show that SPNs receive increased excitatory inputs from within subplate or L5/6 consequent to HI but that the size of individual inputs did not change. Since our

**Table 5** Values for Figure 5

| Area | Comparison (S–C) | Comparison (S–L) | Comparison (C–L) |
|---|---|---|---|
| L4 | $P = 3.86 \times 10^{-3}$ | $P = 0.95$ | $P = 6.60 \times 10^{-4}$ |
| L5/6 | $P = 4.44 \times 10^{-3}$ | $P = 0.10$ | $P = 0.83$ |
| SP | $P = 0.99$ | $P = 0.30$ | $P = 0.19$ |
| Charge | | | |
| L4 | $P = 1.77 \times 10^{-4}$ | $P = 0.91$ | $P = 3.8 \times 10^{-3}$ |
| L5/6 | $P = 3.65 \times 10^{-4}$ | $P = 0.99$ | $P = 1.81 \times 10^{-3}$ |
| SP | $P = 0.02$ | $P = 0.91$ | $P = 3.39 \times 10^{-3}$ |
| Amplitude | | | |
| L4 | $P = 2.52 \times 10^{-4}$ | $P = 0.77$ | $P = 0.02$ |
| L5/6 | $P = 5.58 \times 10^{-3}$ | $P = 0.94$ | $P = 6.43 \times 10^{-4}$ |
| SP | $P = 0.11$ | $P = 0.99$ | $P = 0.27$ |

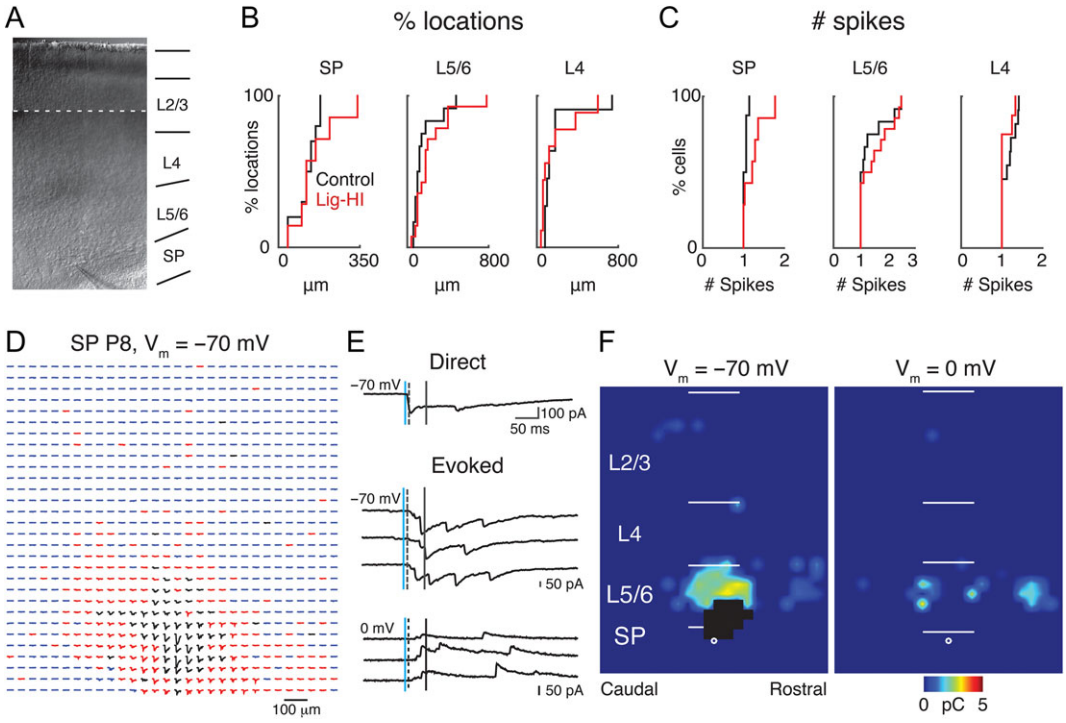


**Figure 2.** LSPS to map intracortical connections to SPNs. (*A*) Infrared image of a thalamocortical brain slice of a P8 rat with a patch pipette on a SPN. Because the ×10 magnification field of view was smaller than the entire brain slice, multiple images were taken along the entire cortical extent into the hippocampal region in order to show the location of the pipette along the rostral-caudal axis with respect to the hippocampus (stitched). (*B*, *C*) Distribution of distance within which 80% of action potentials were evoked (*B*) and number of evoked action potentials (*C*: spike count). (*D*) Traces obtained by LSPS when holding P8 SPN at −70 mV. Traces in black show large-amplitude direct responses. Postsynaptic responses with latencies from 8 to 50 ms are the red traces, and the rest of the traces are in blue. (*E*) Example traces obtained with photostimulation at different locations. The vertical lines on the traces indicate, from left to right, the time of the photostimulation and analysis window. The dashed lines indicate the 8 ms latency after laser onset. (*F*) Pseudocolor maps of a P9 SP neuron show postsynaptic current (PSC) charge at each stimulus location for 1 example subplate neuron. Direct responses in black were discarded from analysis. The white filled circle indicates the location of the soma and the horizontal bars indicate the layer boundaries and serve as scale bars of 200 μm.

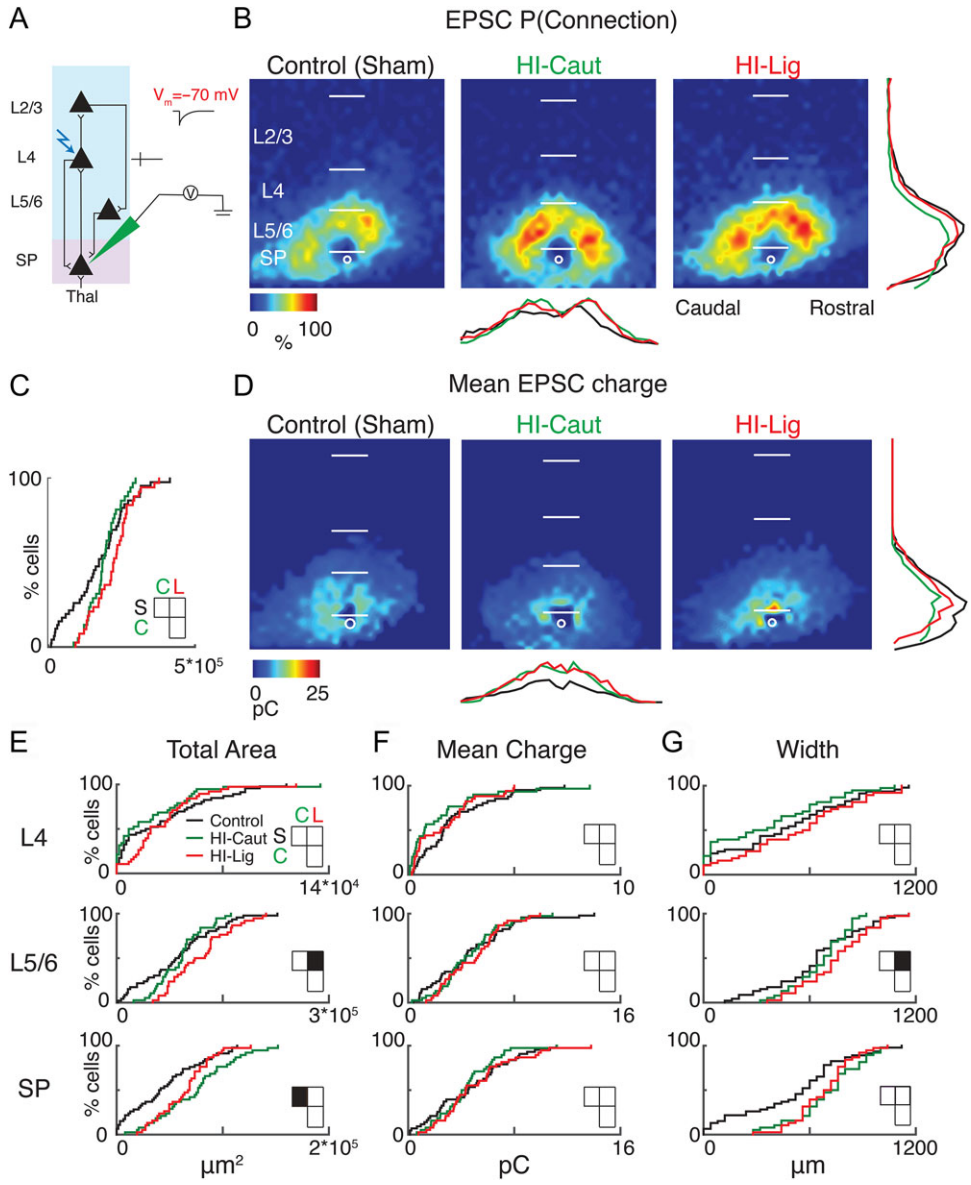


**Figure 3.** HI-Caut results in hyperconnectivity of excitation from SP, while HI-Lig results in hyperconnectivity from L5/6. (*A*) Schematic view of electrode positioning in the layer recorded and laser photostimulation location (photostimulation from pia to SP; see methods for more details). (*B*) Spatial distribution of probability of connection P(Connection) for excitatory (–70 mV) connections. Horizontal bars indicate layer boundaries and serve as scale bar of 200 µm. Black, green, and red overlay traces on the side of the maps indicate summed EPSC marginal distributions for each group. (*C*) Cumulative distribution function (CDF) of excitatory input to SPNs from all layers. Comparisons for S = Control, C = Caut, L = Ligated. Total area: (S–C) $P = 0.80$, (S–L) $P = 0.10$, (C–L) $P = 0.55$. (*D*) Spatial distribution of transferred charge (mean EPSC Charge) for excitatory (–70 mV) connections. (*E–G*) Cumulative distribution function (CDF) of excitatory input to SPNs. Layer totals for area (left), mean transferred charge (middle), and marginal width along rostral-caudal axis (right) for L4, L5/6, and SPN input to the recorded SPN. Black squares in the matrix denote significance, white squares are not significant.

thalamocortical slices preserve the tonotopic axis of A1 along the lateral (columnar) dimension of the slice, the extent of inputs to a particular cell is related to the amount of integration across the different frequency areas of A1. Thus, we analyzed the columnar pattern of the inputs to SPNs by averaging the inputs within each rostro-caudal location and then measured the extent of input in the rostro-caudal direction. Compared with Control, HI-Lig resulted in a wider marginal area of excitatory input from L5/6 to the subplate indicating a larger range of integration across the tonotopic axis (Fig. 3G, Table 3).

Therefore, both HI-Caut and HI-Lig result in hyperconnectivity of excitatory inputs to SPNs. Importantly, while HI-Caut did not cause overt histological changes or SPN loss, we here could detect changes on the functional circuit level. The increase in integration across the tonotopic axis suggests that SPNs receive inputs from a wider range of frequency channels.

## HI-Caut Causes Functional Changes in Inhibitory Subplate Circuits

Hypoxic-Ischemic encephalopathy (HIE) results in variable severity of neuropsychological sequelae. About 25% of the affected infants develop epilepsy and cerebral palsy (Lai and Yang 2011) suggesting that inhibitory circuits might be

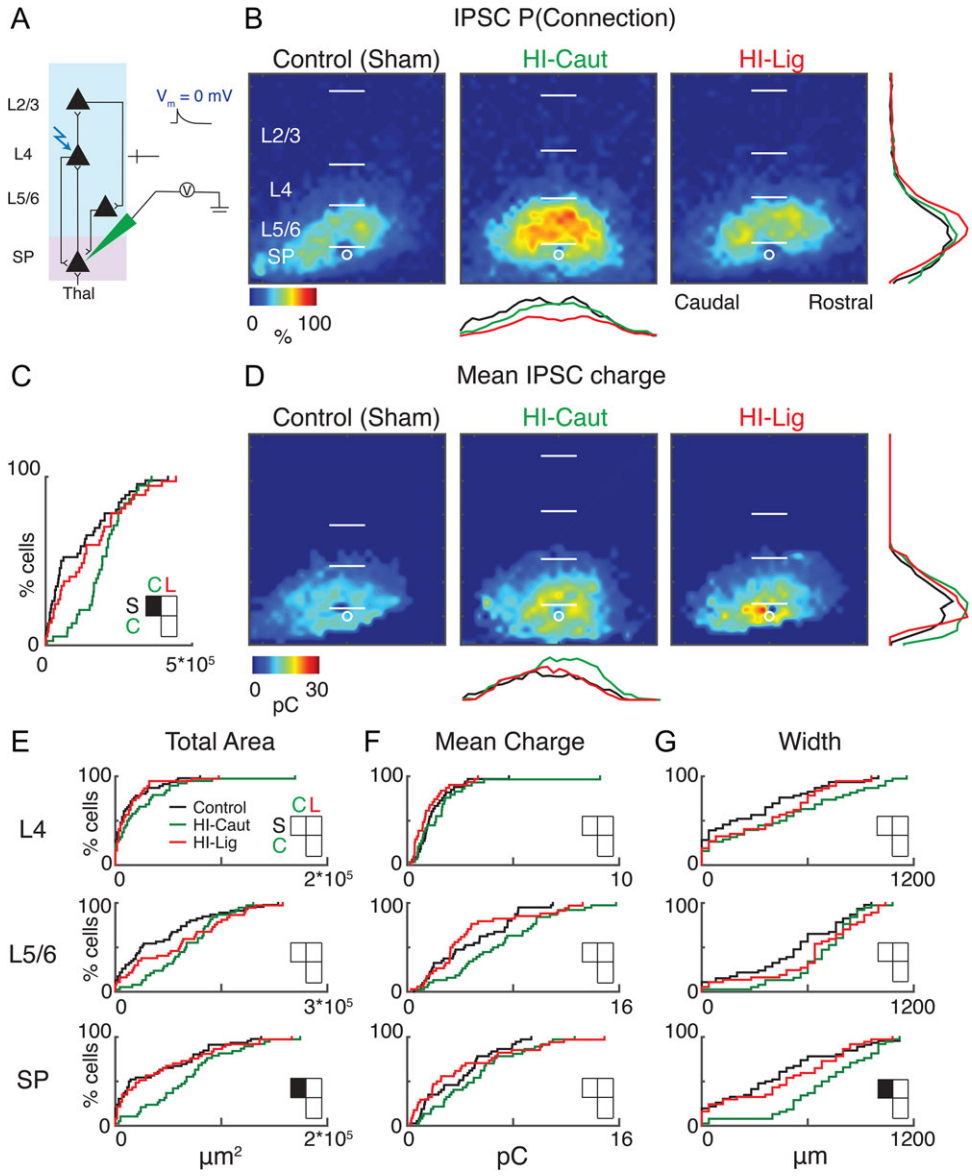


**Figure 4.** HI-Caut results in hyperconnectivity of inhibition in SP. (*A*) Schematic view of electrode positioning in the layer recorded and laser photostimulation location (photostimulation from pia to SP; see methods for more details). (*B*) Spatial distribution of probability of connection P(Connection) for inhibitory (0 mV) connection. Horizontal bars indicate layer boundaries and serve as scale bar of 200 µm. Black, green, and red overlay traces on the side of the maps indicate summed IPSC marginal distributions for each group. (*C*) Cumulative distribution function (CDF) of inhibitory input to SPNs from all layers. Comparisons for S = Control, C = Cauterized, L = Ligated. (*D*) Spatial distribution of transferred charge (Mean IPSC Charge) for inhibitory (0 mV) connections. (*E*–*G*) Cumulative distribution function (CDF) of inhibitory input to SPNs. Layer totals for area (left), mean transferred charge (middle), and marginal width along rostral-caudal axis (right) for L4, L5/6, and SPN input to the recorded SPN.

abnormal. Subplate lesions prevent the maturation of inhibition (Kanold and Shatz 2006) and HI in rodents results in decreased cortical parvalbumin expression levels (Failor et al. 2010). Thus we hypothesized that GABAergic circuits were altered consequent to HI.

To test if the spatial pattern of inhibitory inputs to SPNs was altered, we held cells at 0 mV to isolate inhibitory inputs and performed LSPS (Fig. 4A). HI-Caut but not HI-Lig resulted in a larger total area of inhibitory input (Fig. 4A–C). Laminar analysis revealed that inputs originated from a larger and wider extent of the subplate (Fig. 4B, C, E, G; Table 4). In contrast, HI-Lig did not result in changes to inhibitory connection probability. Neither HI procedure changed the mean IPSC charge (Fig. 4D, F; Table 4). Together, our results show that HI results in hyperconnectivity of excitatory as well as inhibitory circuits. Importantly HI-Caut, which did not cause overt histological defects, resulted in changes on the level of functional excitatory and inhibitory connectivity.

## HI Causes an Excitation/Inhibition Imbalance in Subplate

Our HI procedures caused differential changes in excitatory and inhibitory circuits in SPNs. Since for normal brain function a balance of excitation to inhibition is required, we tested if the combined changes led to an imbalance of excitatory and

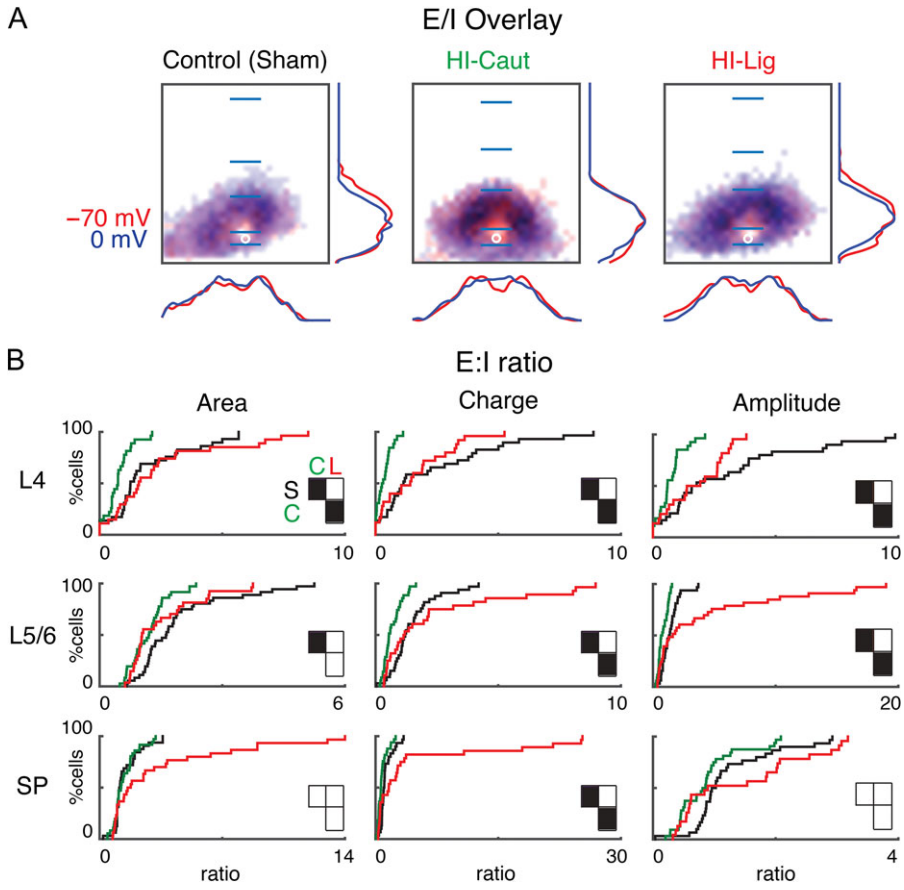


**Figure 5.** Balance of excitatory and inhibitory input to SP for the different conditions. (*A*) Summary schematic of excitatory and inhibitory input probabilities to SPNs superimposed (Control, left; HI-Caut, center; HI-Lig, right). Red color represents excitatory input, and blue color represents inhibitory input to SP. Red and blue overlaying traces on the sides of the maps indicate summed EPSC and IPSC marginal distributions. Blue bars mark layer boundaries and denote 200 μm. (*B*) Cumulative distribution function (CDF) of the ratio of excitatory to inhibitory input as it changes as a result of the different injuries for both area (left), charge (middle), and amplitude (right) for L4, L5/6, and SP.

inhibitory input. We first overlaid the spatial probability maps for excitatory and inhibitory connections (Fig. 5A). Qualitative inspection suggests that connection probability maps under the 3 conditions appear largely coextensive.

To analyze the combined changes in more detail, we calculated for each cell the ratio of the area and charge of the excitatory (AMPA) to inhibitory (GABAergic) input (E/I ratio) for every stimulation site. Compared with Control, HI-Caut resulted in a reduced ratio of E/I for total input area from L4 and L5/6 to SPNs, indicating an unbalanced change of L4 inputs to SPNs that indicates a relative increase in GABAergic inputs (Fig. 5B, Table 5). Since HI-Caut did not cause hyperconnectivity in either excitatory or inhibitory connections from L4 to SPNs, this indicates that there are subtle but consistent changes in both inhibitory and excitatory connections from L4 in individual neurons leading to an E/I imbalance. In contrast, HI-Lig shows no changes in total input area to SPNs indicating that both excitation and inhibition changed in a balanced manner. Calculating the E/I ratio based on the EPSC and IPSC charge or amplitude revealed that similar changes were present in inputs from all layers (Fig. 5B, Table 5). Together, these results show that after HI-Caut, which did not cause morphological deficits on the light microscopic level, GABAergic inputs to SPNs show larger relative hyperconnectivity than glutamatergic inputs. Thus, both HI-Caut and HI-Lig differentially alter inputs to SPNs with GABAergic inputs being affected to a larger degree.

### Hi-Lig Increases the Dendritic Complexity of Subplate Neurons

Our physiological results show hyperconnectivity of intracortical circuits to SPNs after HI. To examine if the reduced functional connectivity is mirrored in the morphological properties of SPNs, we morphologically reconstructed SPNs ($n$ = 25 Ctrl in 7 animals, $n$ = 10 HI-Lig in 3 animals) (Fig. 6A). We found that SPNs in HI-Lig show greater numbers of ends and nodes (Fig. 6B) indicating increased complexity of the dendritic tree consistent with the functional hyperconnectivity. Thus, HI-Lig leads to increases in both dendritic complexity and functional connectivity of SPNs.

## Discussion

Here we show that an animal model of HI causes distinct changes to functional cortical microcircuits to SPNs in the neonatal rodent. In the absence of overt SPN cell loss, the functional circuit changes were pronounced and thus suggest that even mild early HI insults influence SPNs.

Subplate neurons are selectively vulnerable to early excitotoxic injury (Chun and Shatz 1988; Nguyen and McQuillen 2010). HI is an important cause of neonatal brain injury that results from energy failure and excitotoxicity resulting in cell death and inflammation (Ferriero 2004). Variability of injury

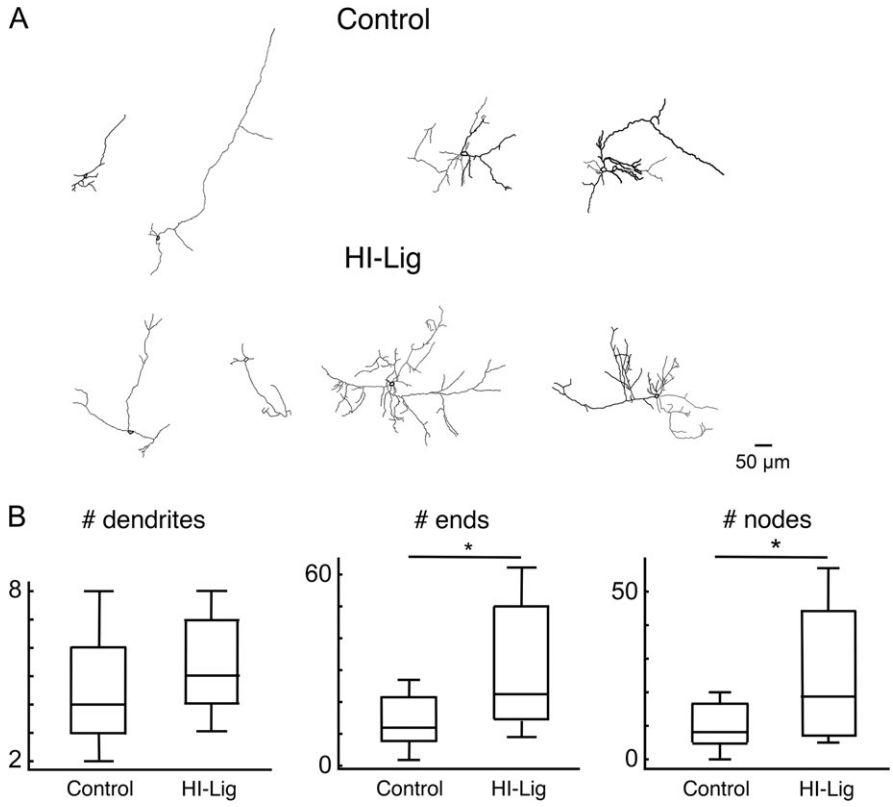


**Figure 6.** SPNs show increased complexity after HI-Lig. (*A*) Exemplar neurolucida reconstructions of recorded SPNs. (*B*) Quantification of morphological properties. Total number of dendrites is unchanged after HI-Lig ($P = 0.19$) while total numbers of ends and nodes are increased after HI-Lig ($P = 0.02$; $P = 0.04$, respectively Rank Sum).

severity is a hallmark of HI brain injury in human newborns. In this study, we show that while the transient and milder HI-Caut did not cause gross histological changes, the more severe HI-Lig could cause gross histological changes that were already detectable in auditory cortex by P5–10. These changes were similar to what has been reported in the visual cortex at P32 (McQuillen et al. 2003; Failor et al. 2010). Nevertheless, we find that in both HI conditions, SPN circuits show hyperconnectivity of excitatory and inhibitory circuits. Moreover, we find that HI-Lig also leads to increased morphological complexity. Thus, SPNs change functionally and anatomically after HI. Therefore, SPN circuits seem to be vulnerable to HI and show circuit changes within a few days after the HI insult. Other insults to the developing brain, such as prenatal valproic acid exposure, also alter SPNs (Nagode et al. 2017). Thus, our results suggest that SPNs form a common target for many neurodevelopmental disorders.

SPNs are amongst the earliest born neurons in the cerebral cortex, and are among the first to receive input from the thalamus as well as from intracortical sources, and project to L4 (Zhao et al. 2009; Kanold and Luhmann 2010; Meng et al. 2014; Viswanathan et al. 2016). Here we show that HI causes an imbalance of excitatory and inhibitory intracortical inputs to SPNs. Thus, the integrative role of SPNs is altered after HI. Since SPNs in sensory cortices can respond to sensory stimuli (Wess et al. 2017) altered connectivity to SPNs likely changes sensory processing. An increase in intracortical excitatory inputs to SPNs would be expected to lead to a relatively decreased functional role of excitatory thalamic inputs. This is consistent with the reduced sensory cortical activation consequent of HI (Ranasinghe et al. 2015).

We find that after HI-Caut, inhibitory inputs to SPNs show relatively larger increases than glutamatergic inputs, leading to decreased E/I ratios. However, the functional effect of this imbalance depends on $E_{Cl}$ which matures in deep cortical layers during the first postnatal week (Shimizu-Okabe et al. 2002). To date, it is unknown how HI affects $E_{Cl}$. Overall, our results show on the cortical microcircuit level, the dynamic and laminar-specific effects of differing severities of HI as a possible substrate for how HI can lead to an imbalance of excitation and inhibition as early as P5–10 which in turn can alter subsequent development.

SPNs take part in the generation of spontaneous cortical oscillations (Dupont et al. 2006), and SPN lesions abolish spindle burst activity in primary somatosensory cortex suggesting that SPNs are a crucial component in the spindle generating or propagating circuit (Tolner et al. 2012). Altered SPN circuits would be expected to alter such a role of SPNs. HI-Lig in rodents resulted in diminished EEG activity (Ranasinghe et al. 2015) consistent with altered SPN circuits and also with altered EEG consequent to HI in human infants (Murray et al. 2009).

Rodent neonatal brain injury models, particularly the Rice-Vannucci HI procedure, have important limitations with respect to human newborn brain injury (Millar et al. 2017). The contribution of HI as a mechanism for brain injury in very premature newborns has been questioned (Gilles et al. 2017). From the standpoint of comparative cortical development, both the rodent subplate layer and mature white matter are diminutive compared with human. Human preterm brain injury is characterized by permanent loss or dysmaturation of myelin, whereas abnormal myelination may only be transient after rodent HI

(Liu et al. 2002). Similarly, the subplate layer in rodents, layer 6b, is very thin throughout development and undergoes comparatively less programmed cell death with persistence of layer 6b in adult animals (Marx et al. 2017). In contrast the subplate zone in humans, at its developmental peak, may be 2–3 times the width of cortical plate and undergoes nearly complete dissolution (Kostovic et al. 2002). The present results should be considered with respect to an appropriate developmental context at the peak of human subplate development from approximately 23 to 29 gestational weeks.

Here we find abnormalities in the functional connectivity of the auditory cortex consequent to HI. Since neonatal HIE in humans is associated with language impairments (Martinez et al. 2014), our results suggest that altered auditory cortex circuits could contribute to these symptoms. Regardless of the severity of the HI, we find that the basic interlaminar circuitry remains intact, indicating that potentially the observed circuit changes, especially after HI-Caut, which did not result in cell loss, might be reversible. Thus, targeted interventions which selectively modulate SPN circuits might be able to reverse the effects of early HI. While the current treatment for HI is hypothermia (Lai and Yang 2011), which presumably reduces activity in all neurons, more efficient treatments might involve targeting different, SPN specific receptors, e.g., neuromodulatory receptors for transmitters such as ACh and serotonin (Hanganu and Luhmann 2004; Kilb et al. 2008; Liao and Lee 2011, 2014).

## Funding

P.O.K. is supported by National Institutes of Health (NIH) R01DC009607. J.P.Y.K. is supported by NIH R01GM056481. A.S. is supported by NIH T32DC000046. P.S.M. is supported by NIH R01NS060896. P.O.K., A.S. designed research. P.O.K. supervised research. J.P.Y.K. contributed reagents. A.S. and J.L. performed surgeries. A.S. performed in vitro experiments. X.M. wrote analysis code for LSPS experiments. A.S., X.M., J.L. performed analysis. A.M. and P.M. performed IHC. A.S., P.O.K. wrote the paper. We thank Dr Amal Isaiah for surgical assistance and Dr Catherine Carr for sharing her Neurolucida system.

## Notes

We thank Andrew Chang, Abanoub Gad, John Krstacic, Kevin Ross, Julia Alexieva, Jacob A. Bart, Shahzeib Syed, and Mathew Thomas for histological assistance. *Conflict of Interest*: The authors declare no conflict of interest.

## References

Barkat TR, Polley DB, Hensch TK. 2011. A critical period for auditory thalamocortical connectivity. Nat Neurosci. 14: 1189–1194.

Chun JJ, Shatz CJ. 1988. Redistribution of synaptic vesicle antigens is correlated with the disappearance of a transient synaptic zone in the developing cerebral cortex. Neuron. 1: 297–310.

Deng R, Kao JPY, Kanold PO. 2017. Distinct translaminar glutamatergic circuits to GABAergic interneurons in the neonatal auditory cortex. Cell Rep. 19:1141–1150.

du Plessis AJ, Volpe JJ. 2002. Perinatal brain injury in the preterm and term newborn. Curr Opin Neurol. 15:151–157.

Dupont E, Hanganu IL, Kilb W, Hirsch S, Luhmann HJ. 2006. Rapid developmental switch in the mechanisms driving early cortical columnar networks. Nature. 439:79–83.

Failor S, Nguyen V, Darcy DP, Cang J, Wendland MF, Stryker MP, McQuillen PS. 2010. Neonatal cerebral hypoxia-ischemia impairs plasticity in rat visual cortex. J Neurosci. 30:81–92.

Ferriero DM. 2004. Neonatal brain injury. N Engl J Med. 351: 1985–1995.

Friauf E, McConnell SK, Shatz CJ. 1990. Functional synaptic circuits in the subplate during fetal and early postnatal development of cat visual cortex. J Neurosci. 10:2601–2613.

Gilles F, Gressens P, Dammann O, Leviton A. 2017. Hypoxia-ischemia is not an antecedent of most preterm brain damage: the illusion of validity. Dev Med Child Neurol. doi: 10.1111/dmcn.13483. [Epub ahead of print].

Hanganu IL, Luhmann HJ. 2004. Functional nicotinic acetylcholine receptors on subplate neurons in neonatal rat somatosensory cortex. J Neurophysiol. 92:189–198.

Higashi S, Hioki K, Kurotani T, Kasim N, Molnar Z. 2005. Functional thalamocortical synapse reorganization from subplate to layer IV during postnatal development in the reeler-like mutant rat (shaking rat Kawasaki). J Neurosci. 25: 1395–1406.

Hoerder-Suabedissen A, Molnar Z. 2015. Development, evolution and pathology of neocortical subplate neurons. Nat Rev Neurosci. 16:133–146.

Hoerder-Suabedissen A, Wang WZ, Lee S, Davies KE, Goffinet AM, Rakic S, Parnavelas J, Reim K, Nicolic M, Paulsen O, et al. 2009. Novel markers reveal subpopulations of subplate neurons in the murine cerebral cortex. Cereb Cortex. 19:1738–1750.

Judas M, Sedmak G, Kostovic I. 2013. The significance of the subplate for evolution and developmental plasticity of the human brain. Front Hum Neurosci. 7:423.

Kanold PO, Kara P, Reid RC, Shatz CJ. 2003. Role of subplate neurons in functional maturation of visual cortical columns. Science. 301:521–525.

Kanold PO, Luhmann HJ. 2010. The subplate and early cortical circuits. Annu Rev Neurosci. 33:23–48.

Kanold PO, Shatz CJ. 2006. Subplate neurons regulate maturation of cortical inhibition and outcome of ocular dominance plasticity. Neuron. 51:627–638.

Kao JP. 2006. Caged molecules: principles and practical considerations. Curr Protoc Neurosci. 6:20. Chapter 6:Unit.

Kilb W, Hanganu IL, Okabe A, Sava BA, Shimizu-Okabe C, Fukuda A, Luhmann HJ. 2008. Glycine receptors mediate excitation of subplate neurons in neonatal rat cerebral cortex. J Neurophysiol. 100:698–707.

Kostovic I, Judas M, Rados M, Hrabac P. 2002. Laminar organization of the human fetal cerebrum revealed by histochemical markers and magnetic resonance imaging. Cereb Cortex. 12: 536–544.

Kostovic I, Rakic P. 1990. Developmental history of the transient subplate zone in the visual and somatosensory cortex of the macaque monkey and human brain. J Comp Neurol. 297: 441–470.

Lai MC, Yang SN. 2011. Perinatal hypoxic-ischemic encephalopathy. J Biomed Biotechnol. 2011:609813.

Liao CC, Lee LJ. 2011. Neonatal fluoxetine exposure affects the action potential properties and dendritic development in cortical subplate neurons of rats. Toxicol Lett. 207:314–321.

Liao CC, Lee LJ. 2014. Presynaptic 5-HT1B receptor-mediated synaptic suppression to the subplate neurons in the somatosensory cortex of neonatal rats. Neuropharmacology. 77:81–89.

Liu Y, Silverstein FS, Skoff R, Barks JD. 2002. Hypoxic-ischemic oligodendroglial injury in neonatal rat brain. Pediatr Res. 51: 25–33.

Martinez C, Carneiro L, Vernier L, Cesa C, Guardiola A, Vidor D. 2014. Language in children with neonatal hypoxic-ischemic encephalopathy. Int Arch Otorhinolaryngol. 18: 255–259.

Marx M, Qi G, Hanganu-Opatz IL, Kilb W, Luhmann HJ, Feldmeyer D. 2017. Neocortical layer 6B as a remnant of the subplate – a morphological comparison. Cereb Cortex. 27: 1011–1026.

McQuillen PS, Ferriero DM. 2005. Perinatal subplate neuron injury: implications for cortical development and plasticity. Brain Pathol. 15:250–260.

McQuillen PS, Sheldon RA, Shatz CJ, Ferriero DM. 2003. Selective vulnerability of subplate neurons after early neonatal hypoxia-ischemia. J Neurosci. 23:3308–3315.

Meng X, Kao JP, Kanold PO. 2014. Differential signaling to subplate neurons by spatially specific silent synapses in developing auditory cortex. J Neurosci. 34:8855–8864.

Mikhailova A, Sunkara N, McQuillen PS. 2017. Unbiased quantification of subplate neuron loss following neonatal hypoxia-ischemia in a rat model. Dev Neurosci. 39:171–181.

Millar LJ, Shi L, Hoerder-Suabedissen A, Molnar Z. 2017. Neonatal hypoxia ischaemia: mechanisms, models, and therapeutic challenges. Front Cell Neurosci. 11:78.

Muralidharan S, Dirda ND, Katz EJ, Tang CM, Bandyopadhyay S, Kanold PO, Kao JP. 2016. Ncm, a photolabile group for preparation of caged molecules: synthesis and biological application. PLoS One. 11:e0163937.

Murray DM, Boylan GB, Ryan CA, Connolly S. 2009. Early EEG findings in hypoxic-ischemic encephalopathy predict outcomes at 2 years. Pediatrics. 124:e459–e467.

Nagode DA, Meng X, Winkowski DE, Smith E, Khan-Tareen H, Kareddy V, Kao JP, Kanold PO. 2017. Abnormal development of the earliest cortical circuits in a mouse model of autism spectrum disorder. Cell Rep. 18:1100–1108.

Nguyen V, McQuillen PS. 2010. AMPA and metabotropic excitoxicity explain subplate neuron vulnerability. Neurobiol Dis. 37:195–207.

Ranasinghe S, Or G, Wang EY, Ievins A, McLean MA, Niell CM, Chau V, Wong PK, Glass HC, Sullivan J, et al. 2015. Reduced cortical activity impairs development and plasticity after neonatal hypoxia ischemia. J Neurosci. 35: 11946–11959.

Robertson CM, Perlman M. 2006. Follow-up of the term infant after hypoxic-ischemic encephalopathy. Paediatr Child Health. 11:278–282.

Segovia KN, McClure M, Moravec M, Luo NL, Wan Y, Gong X, Riddle A, Craig A, Struve J, Sherman LS, et al. 2008. Arrested oligodendrocyte lineage maturation in chronic perinatal white matter injury. Ann Neurol. 63:520–530.

Sheikh A, Meng X, Liu J, Kanold PO. 2017. Neonatal hypoxia-ischemia causes functional intracortical circuit changes in developing auditory cortex. 40th Annual Midwinter Meeting for Association for Research in Otolaryngology. Baltimore, MD.

Shepherd GM, Pologruto TA, Svoboda K. 2003. Circuit analysis of experience-dependent plasticity in the developing rat barrel cortex. Neuron. 38:277–289.

Shimizu-Okabe C, Yokokura M, Okabe A, Ikeda M, Sato K, Kilb W, Luhmann HJ, Fukuda A. 2002. Layer-specific expression of Cl- transporters and differential [Cl-]i in newborn rat cortex. Neuroreport. 13:2433–2437.

Suter BA, O'Connor T, Iyer V, Petreanu LT, Hooks BM, Kiritani T, Svoboda K, Shepherd GM. 2010. Ephus: multipurpose data acquisition software for neuroscience experiments. Front Neural Circuits. 4:100.

Tolner EA, Sheikh A, Yukin AY, Kaila K, Kanold PO. 2012. Subplate neurons promote spindle bursts and thalamocortical patterning in the neonatal rat somatosensory cortex. J Neurosci. 32:692–702.

Viswanathan S, Bandyopadhyay S, Kao JP, Kanold PO. 2012. Changing microcircuits in the subplate of the developing cortex. J Neurosci. 32:1589–1601.

Viswanathan S, Sheikh A, Looger LL, Kanold PO. 2017. Molecularly defined subplate neurons project both to thalamocortical recipient layers and thalamus. Cereb Cortex. 27: 4759–4768. doi: 10.1093/cercor/bhw271.

Volpe JJ. 2012. Neonatal encephalopathy: an inadequate term for hypoxic-ischemic encephalopathy. Ann Neurol. 72:156–166.

Wess JM, Isaiah A, Watkins PV, Kanold PO. 2017. Subplate neurons are the first cortical neurons to respond to sensory stimuli. Proc Natl Acad Sci U S A. 114:12602–12607. doi:10.1073/pnas.1710793114.

Zhang LI, Bao S, Merzenich MM. 2001. Persistent and specific influences of early acoustic environments on primary auditory cortex. Nat Neurosci. 4:1123–1130.

Zhao C, Kao JP, Kanold PO. 2009. Functional excitatory microcircuits in neonatal cortex connect thalamus and layer 4. J Neurosci. 29:15479–15488.